Nuclear Engineering and Technology 51 (2019) 843–852

Contents lists available at ScienceDirect

Nuclear Engineering and Technology

journal homepage: www.elsevier.com/locate/net

Original Article

Dose coefficients of mesh-type ICRP reference computational phantoms for idealized external exposures of photons and electrons

Yeon Soo Yeom [a], Chansoo Choi [b], Haegin Han [b], Hanjin Lee [b], Bangho Shin [b], Thang Tat Nguyen [c], Min Cheol Han [d], Choonsik Lee [a], Chan Hyeong Kim [b, *]

[a] Division of Cancer Epidemiology & Genetics, National Cancer Institute, National Institute of Health, 9609 Medical Center Drive, Bethesda, MD, 20850, USA
[b] Department of Nuclear Engineering, Hanyang University, 222 Wangsimni-ro, Seongdong-gu, Seoul, 04763, Republic of Korea
[c] School of Nuclear Engineering and Environmental Physics, Hanoi University of Science and Technology, 1 Dai Co Viet Road, Hai Ba Trung District, Hanoi, Viet Nam
[d] INFN Sezione di Genova, Via Dodecaneso 33, Genova, 16146, Italy

ARTICLE INFO

Article history:
Received 17 September 2018
Accepted 11 December 2018
Available online 13 December 2018

Keywords:
Dose coefficients
ICRP
Reference phantoms
Mesh
Monte Carlo
Geant4

ABSTRACT

In the present study, we established a comprehensive dataset of dose coefficients (DCs) of the new mesh-type ICRP reference computational phantoms (MRCPs) for idealized external exposures of photons and electrons with the Geant4 code. Subsequently, the DCs for the nine organs/tissues, calculated for their thin radiosensitive target regions, were compared with the values calculated by averaging the absorbed doses over the entire organ/tissue regions to observe the influence of the thin sensitive regions on dose calculations. The result showed that the influences for both photons and electrons were generally insignificant for the majority of organs/tissues, but very large for the skin and eye lens, especially for electrons. Furthermore, the large influence for the skin eventually affected the effective dose calculations for electrons. The DCs of the MRCPs also were compared with the current ICRP-116 values produced with the current ICRP-110 reference phantoms. The result showed that the DCs for the majority of organs/tissues and effective dose were generally similar to the ICRP-116 values for photons, except for very low energies; however, for electrons, significant differences from the ICRP-116 values were found in the DCs, particularly for superficial organs/tissues and skeletal tissues, and also for effective dose.

1. Introduction

The International Commission on Radiological Protection (ICRP), following the 2007 Recommendations in ICRP Publication 103 [1], has provided the reference values of dose coefficients (DCs) for external radiation exposures in ICRP Publication 116 [2]. The ICRP-116 DCs were produced by performing Monte Carlo particle transport simulations coupled with the adult male and female reference computational phantoms described in ICRP Publication 110 [3]. The ICRP-110 reference phantoms, which represent the Reference Adult Male and Female established in ICRP Publication 89 [4], are voxel models based on computed tomography images of real persons; as such, they provide a more realistic representation of the human anatomy than do the previous stylized models based on simple mathematical equations.

However, the ICRP-110 voxel phantoms are inadequate for representing organs/tissues of small and/or thin structure below the dimensions of the voxel sizes (male: $2.137 \times 2.137 \times 8.0$ mm^3 and female: $1.775 \times 1.775 \times 4.8$ mm^3). For example, in the ICRP-110 phantoms, the walls of some organs/tissues (e.g., skin, gall bladder, urinary bladder, and gastrointestinal tract) are discontinuous, which can result in unreliable dose calculations particularly for weakly penetrating radiation. Similarly, the eye lens is not fully covered by the cornea and aqueous humor; thus, radiation can directly reach it through the openings in the cornea and aqueous humor. Therefore, the ICRP-116 lens DCs were calculated for some electron exposure cases [2] using a supplemental stylized eye model developed by Behrens et al. [5]. Moreover, the micron-scale radiosensitive target regions considered in the ICRP, e.g., the 50-μm-thick basal layer of the skin [2] and 8–40-μm-thick stem cell layers of the respiratory and alimentary tract systems [6–8], are not modeled in the ICRP-110 phantoms. The ICRP-116 DCs for these organs/tissues were calculated using dose approximation, i.e., by averaging the absorbed doses over the entire organ/tissue regions

* Corresponding author.
E-mail address: chkim@hanyang.ac.kr (C.H. Kim).

https://doi.org/10.1016/j.net.2018.12.006

of the phantoms. Also, the specific absorbed fractions (SAFs) of ICRP Publication 133 [8] for the respiratory and alimentary tract systems for charged particles were calculated using additional supplementary organ/tissue-specific stylized phantoms.

To address these limitations, the ICRP formed Task Group 103 with the objective of developing new mesh-type reference computational phantoms (MRCPs). Recently, this task group completed the development of the MRCPs for the adult male and female, which are the mesh counterparts of the voxel-type ICRP-110 reference phantoms [9,10]. The adult MRCPs were constructed by converting the ICRP-110 voxel phantoms into a high-quality mesh format and simultaneously overcoming the limitations of the voxel phantoms due to their limited voxel resolutions. The new mesh phantoms include all the target and source regions relevant to dose assessment for radiological protection purposes, even micron-scale regions of the respiratory and alimentary tract systems, skin, eye lens, and urinary bladder, thereby, eliminating the requirement for supplementary stylized phantoms.

In the present study, we used the MRCPs to establish a comprehensive dataset of DCs for the ideal external exposures of photons and electrons by performing Monte Carlo dose calculations with the Geant4 code [11]. The calculated values are dose coefficients for organ/tissue absorbed dose (DC_T`s) for 30 individual organs/tissues and dose coefficients for effective dose ($DC_E$`s) for a wide range of energies (0.01 MeV–10 GeV) in six irradiation geometries (i.e., antero-posterior (AP), postero-anterior (PA), left-lateral (LLAT), right-lateral (RLAT), rotational (ROT), and isotropic (ISO)) for photons and in three geometries (AP, PA, and ISO) for electrons. Subsequently, to investigate the dosimetric influence of the thin radiosensitive regions defined in the MRCPs, the produced DC_T`s for the organs/tissues that include the sensitive regions were compared with the values calculated using the conventional dose approximation based on the entire regions. Additionally, the DCs of the MRCPs were compared with the ICRP-116 DCs [2] that had been produced with the current voxel-type ICRP-110 reference phantoms, in order to see the dosimetric influence of the improved representation of the organs/tissues in the MRCPs.

2. Materials and methods

2.1. ICRP adult mesh-type reference computational phantoms

Fig. 1 shows the adult male and female MRCPs along with the voxel-type ICRP-110 reference phantoms. The majority of the organs/tissues of the MRCPs were constructed by directly converting the ICRP-110 phantoms into a high-quality mesh format (i.e., a perfect mesh geometry without abnormal facets and that can be implemented in Monte Carlo codes) via 3D surface rendering and several refinement procedures [9,12]. Several organs/tissues in structures that were too complex and/or small, to which the direct conversion approach therefore was inapplicable, were constructed using certain modeling approaches [13–16]. One such example is the eyes, which were constructed by reproducing the stylized eye model of Behrens et al. [5] in mesh format [13]. Another example is the small intestines, which were constructed using a systematic modeling procedure developed based on a Monte Carlo approach [14]. The masses of the organs and tissues were matched to the reference values that are inclusive of blood content [4,8], as a large amount of blood is situated in the small vessels and capillaries that are distributed in the organs/tissues. The body heights and weights of the phantoms were also matched to the reference values (male: 1.76 m and 73 kg; female: 1.63 m and 60 kg) [4]. All of the micron-scale radiosensitive target and source regions of the respiratory and alimentary tract systems, skin, and urinary bladder were defined in the MRCPs [10,16,17]. The male MRCP comprised 2.5 million triangular facets in the polygon-mesh (PM) format and 8.2 million tetrahedrons in the tetrahedral-mesh (TM) format. The female MRCP comprised 2.6 million triangular facets in the PM format and 8.6 million tetrahedrons in the TM format. The TM-format MRCPs were converted from the PM-format MRCPs via tetrahedralization using the TetGen code [18].

2.2. Monte Carlo dose calculations

Monte Carlo particle transport simulations were performed with the MRCPs to calculate the DCs for ideal external exposures of photons and electrons. For this, the MRCPs in the TM geometry were implemented in the Geant4 Monte Carlo code (ver. 10.04) via the G4Tet class following the procedure used in Yeom et al. [19]. It should be noted that the PM geometry can also be implemented in the Geant4 code via the *G4TessellatedSolid* class; however, the computation speed for the PM geometry is significantly lower than that for the TM geometry [19]. The airway models representing bronchi and bronchioles in the constructive solid geometry format were implemented in the Geant4 code using the *G4VUserParallelWorld* class, as per the procedure used in Kim et al. [16]. Fig. 2 shows the MRCPs implemented in the Geant4 code.

Next, monoenergetic broad parallel beams of photons and electrons with energies ranging from 10 keV to 10 GeV were used for the whole-body irradiation of the phantoms in the ideal irradiation geometries. In the present study, as considered in ICRP Publication 116 [2], the six irradiation geometries (i.e., antero-posterior (AP), postero-anterior (PA), left-lateral (LLAT), right-lateral (RLAT), rotational (ROT), and isotropic (ISO)) were calculated for the photons, and the three irradiation geometries (i.e., AP, PA, and ISO) were calculated for the electrons. To generate a parallel beam, a 2-m-diameter disk that uniformly emits particles in its normal direction, incident to the whole body of the phantoms, was modeled by using the *G4GeneralParticleSource* class. Additionally, a 30-cm-diameter parallel beam incident to the head of the phantoms was modeled for the calculation of the lens doses in order to save computation time, under the assumption that the contribution of the secondary radiations (from the other parts of the body) to the eye lens dose is negligible [13].

The DC_T in terms of absorbed dose per fluence (pGy cm^2) were calculated using the equation:

$$DC_T = D_T\left(\frac{A}{N}\right) \quad (1)$$

where D_T is the organ dose (= organ/tissue-averaged absorbed dose, pGy) for the organ/tissue T, A is the area (cm^2) of the disk source, and N is the number of primary particles emitted from the disk source. The absorbed doses for all of the organs/tissues, with some exceptions, were directly calculated from the MRCPs using the *G4PSEnergyDeposit* class. The exceptions were the absorbed doses for red bone marrow (RBM) and bone surface (also called endosteum; total marrow within 50-μm thickness of bone surface), which are implicitly represented in the MRCPs as in the ICRP-110 reference phantoms [15]. Therefore, these skeletal absorbed doses were calculated using two estimates introduced in ICRP Publication 116 [2].

The skeletal doses for the electrons were calculated using the equations:

$$D_{RBM} = \sum_x \frac{m^x_{RBM}}{m^{total}_{RBM}} D^x_{SP} \quad (2)$$

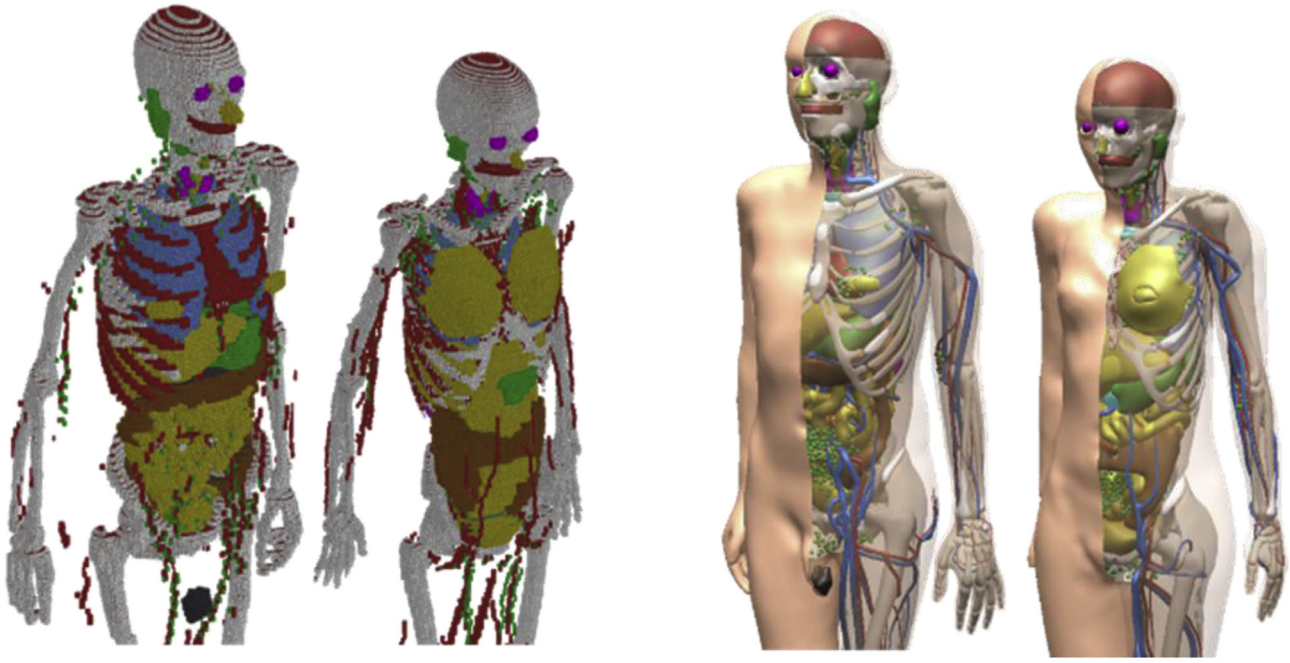

Fig. 1. Mesh-type ICRP adult reference phantoms (right) along with voxel-type ICRP adult reference phantoms (left).

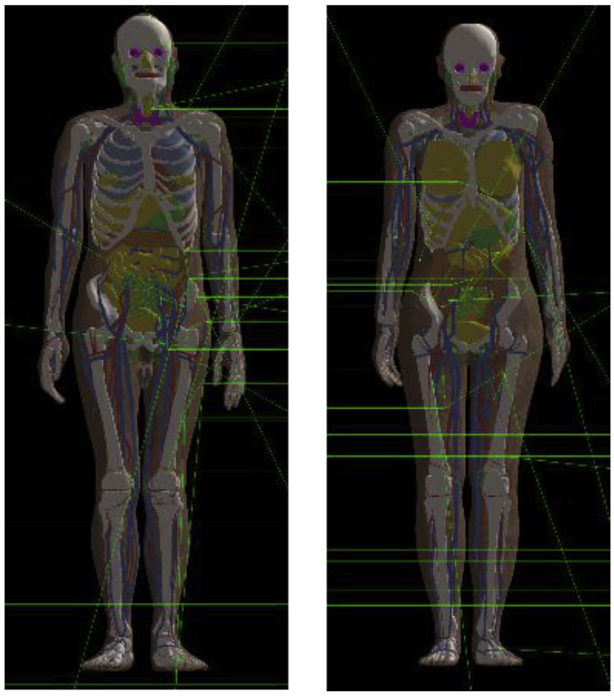

Fig. 2. Adult male (left) and female (right) mesh-type ICRP reference phantoms implemented in Geant4 code.

$$D_{TM_{50}} = \sum_x \frac{m^x_{TM_{50}}}{m^{total}_{TM_{50}}} D^x_{SP} + \sum_x \frac{m^x_{TM_{50}}}{m^{total}_{TM_{50}}} D^x_{MM} \quad (3)$$

where D_{RBM} and $D_{TM_{50}}$ are the absorbed doses to the RBM and endosteum, respectively; m^x_{RBM} and $m^x_{TM_{50}}$ are the masses of these tissues at bone site x, respectively; m^{total}_{RBM} and $m^{total}_{TM_{50}}$, respectively, are the masses of these tissues summed across the entire skeleton; D^x_{SP} and D^x_{MM} are the absorbed doses to the spongiosa and medullary cavity, respectively, at bone site x of the phantoms. Note that the masses of the RBM and endosteum at each bone site are provided in ICRP Publication 116 [2]. This approach was used to calculate the skeletal doses for the photons with energies higher than 10 MeV. For lower energy photons, whereas the same approach was consistently used in the calculation of the ICRP-116 skeletal DCs, in the present study, a more advanced approach was used based on the fluence-to-absorbed dose response functions (DRFs) developed by Johnson et al. [20] and provided in ICRP Publication 116 [2]. For this calculation, the scoring class derived from the *G4VPrimitiveScorer* class [15] was used to convert the fluence values in the regions of the spongiosa or medullary cavity at a given photon energy to the corresponding skeletal doses via a log–log interpolation of the DRF values.

For the organs/tissues that include radiosensitive target regions (i.e., the extrathoracic (ET) region, lungs, oesophagus, stomach, small and large intestines, skin, eye lens, and urinary bladder), additional DC_T`s were calculated without considering the sensitive region, i.e., by averaging the absorbed dose over the entire region, for the purpose of comparison.

The calculated DC_T`s for all of the organs/tissues were then used to calculate the $DC_E$`s in terms of effective dose per fluence (pSv cm^2) using the equation:

$$DC_E = \sum_T w_T \sum_R w_R \left(\frac{DC^{Male}_{T,\ R} + DC^{Female}_{T,R}}{2} \right) \quad (4)$$

where $DC_{T,R}$ is the dose coefficient of the organ/tissue T and radiation R, w_T is the tissue-weighting factor, and w_R is the radiation-weighting factor. The tissue- and radiation-weighting factors are given in ICRP Publication 103 [1].

The number of primary particles varied from 10^8 to 10^{10} depending on the particles and energies. The physics library of *G4EmLivermorePhysics* was applied for the transport of photons and electrons. For the electrons with energies less than 10 MeV, the bremsstrahlung splitting technique was used with a splitting factor

of 10–1000 depending on the energies in order to enhance the production of bremsstrahlung photons. Considering the micron scales of the thin radiosensitive regions in the MRCPs, the range value of 1 μm for the secondary production cut was applied to both photons and electrons. The simulations were performed on Biowulf, the National Institute of Health's high-performance Linux computing cluster (http://hpc.nih.gov). The statistical relative errors for the calculated DC_E`s were all less than 0.5%, and the majority of the calculated $DC_T$`s were less than 1%.

3. Results and discussion

3.1. Dose coefficients for photons and electrons

Comprehensive data on the DCs of the MRCPs for external exposures of photons and electrons were calculated by performing Monte Carlo dose calculations with the Geant4 code. The data include DC_T`s in terms of organ dose per fluence (pGy cm^2) for 30 organs/tissues (i.e., RBM, colon, lung, stomach, breast, testes, ovaries, urinary bladder, oesophagus, liver, thyroid, endosteum, brain, salivary glands, skin, adrenals, ET region, gall bladder, heart, kidneys, lymphatic nodes, muscle, oral mucosa, pancreas, prostate, small intestine, spleen, thymus, uterus, and eye lens) and DC_E`s in terms of effective dose per fluence (pSv $cm^2$). Note that the $DC_T$`s for the nine organs/tissues (i.e., colon, lungs, stomach, urinary bladder, oesophagus, skin, ET region, small intestine, and eye lens) that include thin radiosensitive target regions were calculated by averaging the absorbed doses over only the sensitive regions, not the entire organ/tissue regions. The photon DCs were obtained for 55 energy values ranging from 0.01 MeV to 10 GeV and six irradiation geometries (AP, PA, LLAT, RLAT, ROT, and ISO). The electron DCs were obtained for 49 energy values ranging from 0.01 MeV to 10 GeV and three irradiation geometries (AP, PA, and ISO). The numerical values of all of the DCs are tabulated in the Supplementary Data tables available online.

Fig. 3 shows the photon and electron DC_E`s for the considered irradiation geometries. For photons, the $DC_E$`s tend to increase monotonically with energy over the entire energy region for all geometries. Also, the DC_E`s for the different geometries tend to differ over the entire energy region. For energies <10 MeV, the $DC_E$`s of the AP geometry are greater than those of the other geometries, the maximum difference being a factor of approximately nine relative to the value of the PA geometry at 0.02 MeV. On the other hand, for high energies, the DC_E`s of the AP geometry are lower than those of the other geometries, the maximum difference being a factor of approximately three relative to the value of the ISO geometry at the highest energy (10 GeV).

For electrons, the DC_E`s also tend to increase with energy but show more complicated variations. It can be observed that the $DC_E$`s at energies from 0.05 to 0.1 MeV dramatically increase with energy, i.e., by about four orders of magnitude. Meanwhile, the DC_E`s at energies from 0.15 to 0.8 MeV decrease with energy. The $DC_E$`s of the different geometries also can be seen to be significantly different at energies from 0.8 to 30 MeV, where the AP geometry shows the highest values and the PA geometry shows the lowest values. The maximum difference between the AP and PA geometries is approximately 15 times at 4 MeV.

3.2. Dosimetric influence of radiosensitive regions

In the present study, the DC_T`s of the nine organs/tissues including micron-scale radiosensitive regions were compared with those calculated by averaging the absorbed dose over the entire organ/tissue region in order to observe the influence of the sensitive regions defined in the MRCPs on dose calculations.

Fig. 4 show the ratios of the DC_T`s based on the sensitive region with respect to the values based on the entire region for photons in the AP, PA, and ISO geometries. For all organs/tissues except the eye lens and skin, the DC_T ratios tend to be close to unity over the entire energy region (i.e., mostly between 0.9 and 1.1), which means that the influence of the sensitive regions on dose calculations is generally not significant. Large deviations from unity are found only at low energies (i.e., <0.03 MeV) for most organs/tissues, due to the fact that the low-energy photons with weakly penetrating powers establish large dose gradients within the organs/tissues. For the eye lens, the ratios at energies >1 MeV in the AP geometry are significantly lower than unity (i.e., mostly ~ 0.7); that is, the lens DC_T`s based on the sensitive regions are 30% lower than those based on the entire region. For the skin, the DC_T ratios at the energies from 0.3 to 20 MeV are significantly lower than unity, with a minimum value of approximately 0.7 at 0.8 MeV. These significant differences for the eye lens and skin — even for such high-energy photons with highly penetrating powers — is due to the fact that charged particle equilibrium is not well established in these superficial tissues.

Fig. 5 shows the results for electrons. For all organs/tissues except for the eye lens and skin, the ratios tend to be close to unity over the entire energy region (i.e., mostly between 0.9 and 1.1), while relatively large deviations from unity are observed in some cases at energies from 2 to 10 MeV. For the eye lens, the ratios in the PA geometry tend to be close to unity over the entire energy region,

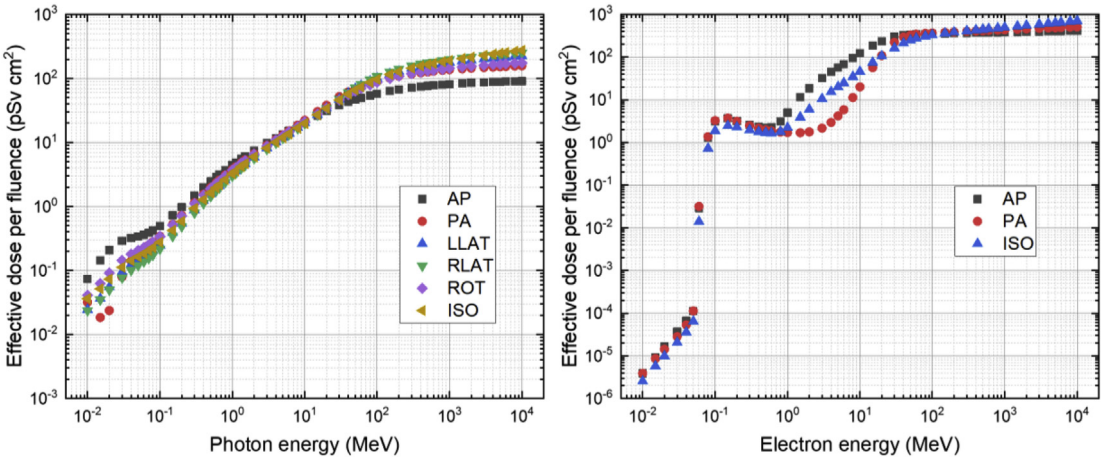

Fig. 3. Effective dose per fluence (pSv cm^2) calculated with MRCPs and Geant4 code for photons (left) and electrons (right).

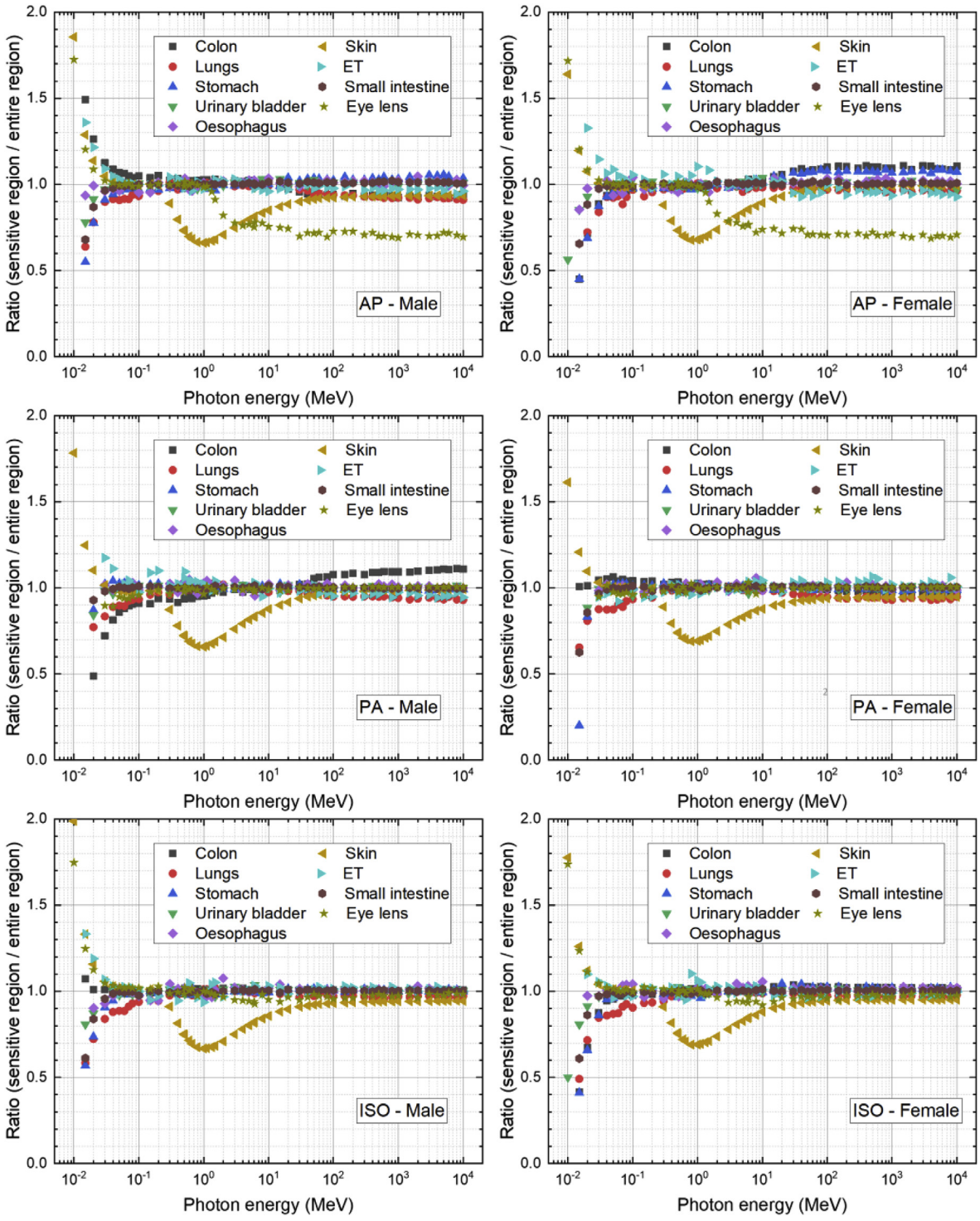

Fig. 4. Ratios of DC_T`s based on sensitive region with respect to the values based on entire region for colon, lungs, stomach, urinary bladder, oesophagus, skin, ET region, small intestine, and eye lens of male (left) and female (right) MRCPs for photons in AP, PA, and ISO geometries.

but the ratios in the AP and ISO geometries at energies <2 MeV are significantly greater than unity, with a maximum value of 4.4 at 0.8 MeV in both geometries. This means that the lens DC_T`s based on the sensitive region are up to 4.4 times higher than those based on the entire region in the AP and ISO geometries, which are considered to be important in the lens dose calculation. For the skin, it can be seen that for all of the geometries, the ratios at energies <1 MeV are significantly different from unity. The ratios at energies $\leq$0.06 MeV are less than unity by up to approximately four orders of magnitude at the lowest energy (0.01 MeV). By contrast, the ratios at the higher energies are greater than unity by up to approximately an order of magnitude at 0.1 MeV.

3.2.1. *Dose coefficients for effective dose*

The influence of the sensitive regions on effective dose calculations was also investigated. For this, the DC_E`s based on the

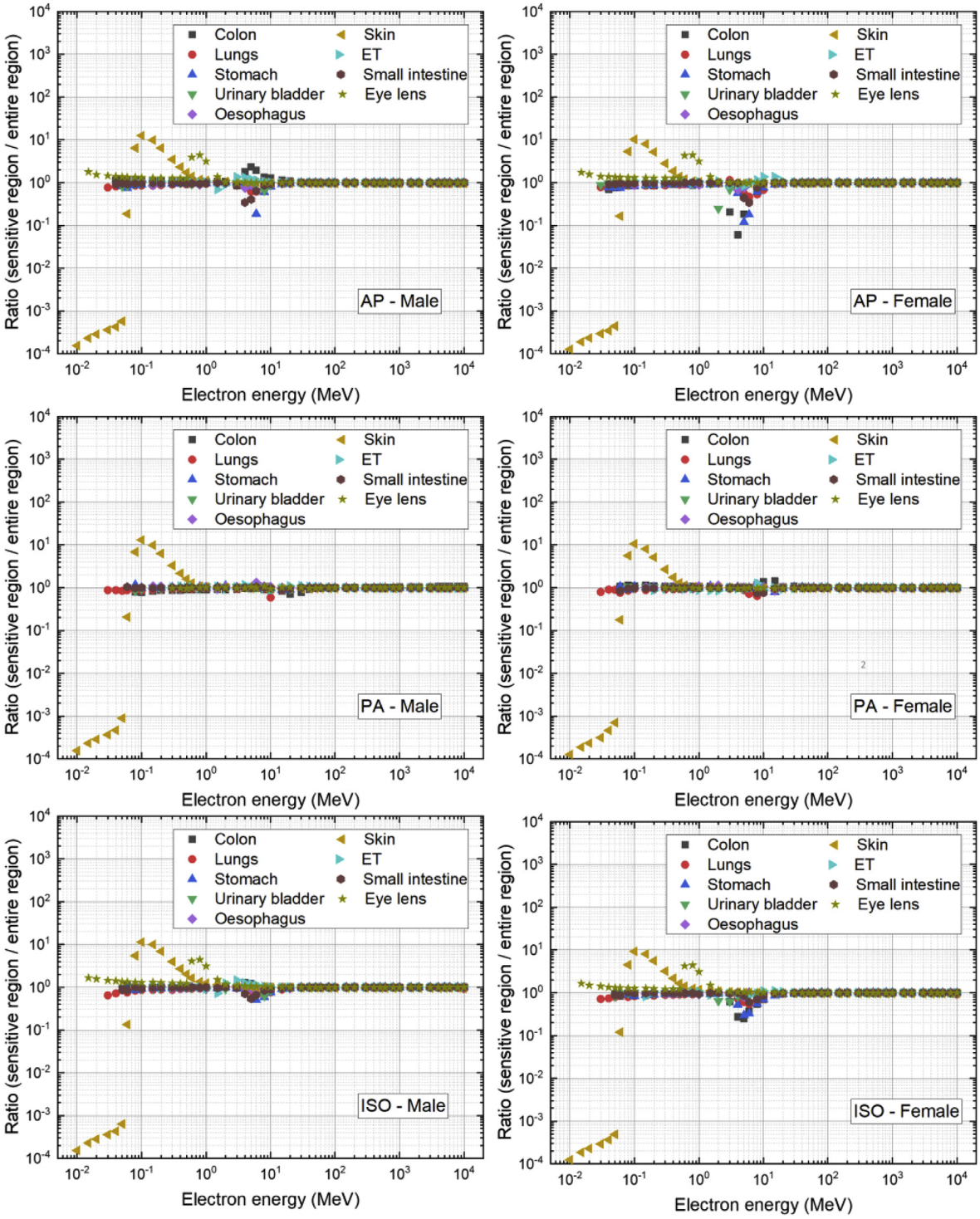

Fig. 5. Ratios of DC_T`s based on sensitive region with respect to values based on entire region for colon, lungs, stomach, urinary bladder, oesophagus, skin, ET region, small intestine, and eye lens of male (left) and female (right) MRCPs for electrons in AP, PA, and ISO geometries.

sensitive regions were compared with the values based on the entire regions. Fig. 6 shows the ratios of the DC_E`s based on the sensitive regions with respect to the values based on the entire regions for photons and electrons and the irradiation geometries considered in the present study.

For photons, the ratios tend to be close to unity over the entire energy region (i.e., mostly between 0.99 and 1.01), which indicates that the influence of the sensitive regions on the effective dose calculations is generally not significant. Only at very low energies (<0.03 MeV), the ratios show relatively large deviations from unity, the maximum ratio being 1.7 at the lowest energy (0.01 MeV) in the PA geometry. These differences in DC_E`s are mainly influenced by the dose differences due to the skin sensitive region rather than the other organ/tissue sensitive regions. The low-energy photons with weakly penetrating powers deposit most of their energies at the skin and, thus, the skin doses mainly contribute to effective dose

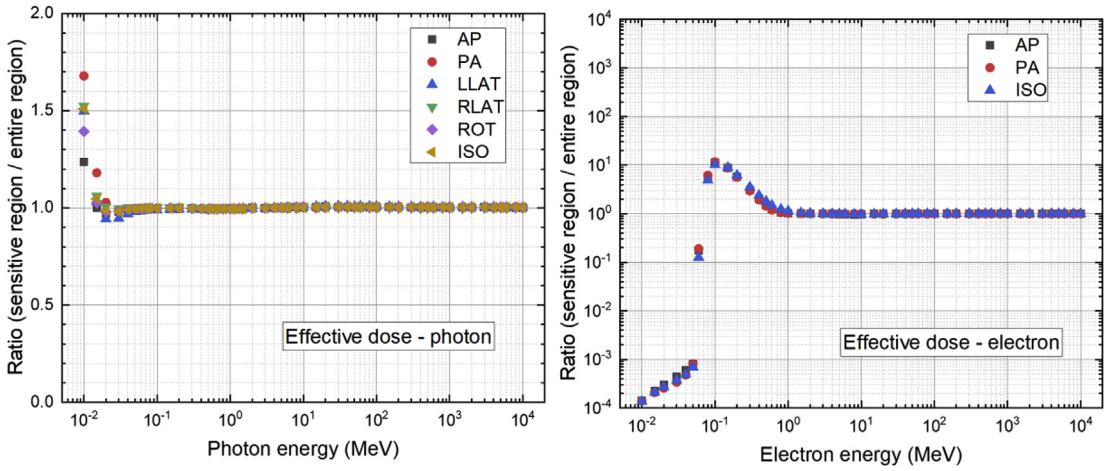

Fig. 6. Ratios of DC_E`s of MRCPs based on sensitive region with respect to values based on entire region for photons (left) and electrons (right).

despite the small tissue-weighting factor (= 0.01) (ICRP 2007).

For electrons, the ratios at energies >1 MeV tend to be close to unity (i.e., mostly between 0.99 and 1.01), whereas those at the lower energies are significantly different from unity. It can be observed that the ratios are almost identical to those for the skin, as shown in Fig. 5, which indicates that these differences are mainly influenced by the skin dose differences due to the skin sensitive region. These primary electrons at energies ≤1 MeV deposit most of their energies to the skin, whereas very-low-energy secondary photons (e.g., bremsstrahlung photons) mostly contribute to the doses to the other organs/tissues; therefore, the skin dose is the main contributor to the effective dose.

3.3. Comparison with ICRP-116 dose coefficients

The presented DCs of the MRCPs were compared with the current reference values in ICRP Publication 116 [2] produced with the voxel-type ICRP-110 reference phantoms [3] in order to observe the dosimetric influence of the improved representation of the organs/tissues of the MRCPs as compared with the ICRP-110 phantoms.

3.3.1. Dose coefficients for organ/tissue absorbed dose

Fig. 7 shows the ratios of the DC_T`s of the MRCPs with respect to the ICRP-116 $DC_T$`s for 15 organs/tissues (RBM, colon, lungs, stomach, breasts, remainder tissues, gonads, urinary bladder, oesophagus, liver, thyroid, endosteum, brain, salivary glands, and skin) for photons in the ISO geometry. It should be noted that the DC_T`s for the remainder tissues are the arithmetic mean values for the 13 organs/tissues (i.e., adrenals, ET region, gall bladder, heart, kidneys, lymphatic nodes, muscle, oral mucosa, pancreas, prostate (male)/uterus (female), small intestine, spleen, and thymus), as defined in ICRP Publication 103 [1].

For all organs/tissues, with the exception of the skeletal tissues and skin, the ratios tend to be close to unity over the entire energy region (i.e., mostly between 0.9 and 1.1), which means that the MRCP DC_T`s for these organs/tissues are similar to the ICRP-116 $DC_T$`s. Only at very low energies (<0.03 MeV), the ratios show relatively large deviations from unity, which was observed mainly owing to the difference in geometry or material composition between the MRCPs and ICRP-110 phantoms. For the skeletal tissues (RBM and endosteum), the ratios at energies > 0.1 MeV are close to unity, whereas those at lower energies are significantly smaller than unity, i.e., by up to approximately two or three orders of magnitude at the lowest energy (0.01 MeV). These significant differences were observed mainly because of two reasons: (1) the cortical bones in the ICRP-110 phantoms, due to the limited voxel resolutions, do not fully cover the spongiosa and medullary-cavity regions, while this limitation was eliminated in the MRCPs; (2) the MRCP DC_T`s for these skeletal tissues were calculated using the DRFs [20], whereas the ICRP-116 values were calculated using a simpler method, i.e., Equations (2) and (3) in Section 2.2. For the skin, the ratios at energies >10 MeV are close to unity, whereas those at lower energies showed relatively large deviations from unity. These deviations were observed mainly because the MRCP skin DC_T`s were calculated using the skin sensitive region of the MRCPs, whereas the ICRP-116 values were calculated using the entire region of the skin of the ICRP-110 phantoms, which, owing to their limited voxel resolutions, do not include the thin sensitive regions.

Fig. 8 shows the results for the electrons. At energies >10 MeV, the ratios tend to be close to unity (i.e., mostly between 0.9 and 1.1). At lower energies, the ratios for some organs/tissues (colon, lungs, stomach, urinary bladder, oesophagus, liver, thyroid, and brain) are also close to unity in most cases, while relatively large differences from unity can be observed in some other cases at energies from 2 to 10 MeV. For the other organs/tissues (i.e., skin, breasts, gonads, salivary glands, remainder tissues, RBM, and endosteum), the ratios are significantly different from unity in the majority of cases. For the skin, the ratios at energies ≤0.06 MeV are significantly less than unity, whereas those at the higher energies are significantly greater than unity. The ratios are also almost identical to the ratios of the MRCP sensitive-region-averaged skin dose and the MRCP entire-region-averaged skin dose, as shown in Fig. 5, which indicates that the deviations from the ICRP-116 values are mainly due to the use of the skin sensitive region in the MRCPs. For the superficial organs/tissues (breasts, gonads, and salivary glands), the ratios are significantly smaller than unity, i.e., by several orders of magnitude, which means that the MRCP DCs are significantly lower than the ICRP-116 values. These differences were observed mainly owing to the improved representation of the organs/tissues in the MRCPs as compared with the ICRP-110 voxel phantoms. That is, the skin of the ICRP-110 phantoms, due to the limited voxel resolutions, is discontinuous, and thus, electrons without energy loss in the skin can directly deposit their energies to these superficial organs/tissues. This limitation is eliminated in the MRCPs. This improvement also results in significant deviations from the ICRP-116 values for the remainder tissues, of which some organs/tissues such as the muscle and lymphatic nodes of the ICRP-110 phantoms are also

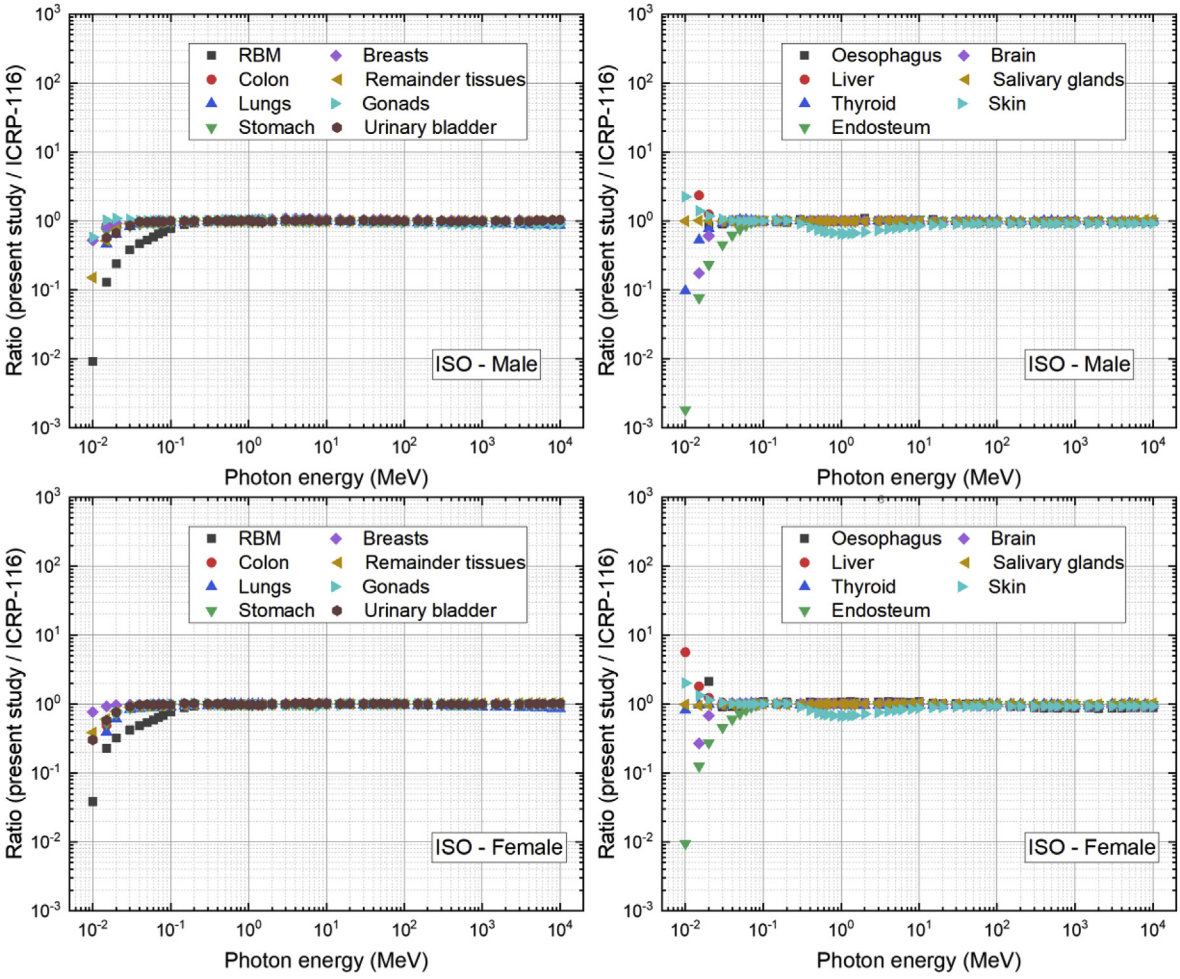

Fig. 7. Ratios of MRCP DC_T`s calculated in present study with respect to ICRP-116 DC_T (ICRP 2010) for RBM, colon, lungs, stomach, breasts, remainder tissues, gonads, urinary bladder, oesophagus, liver, thyroid, endosteum, brain, salivary glands, and skin for photons in ISO geometry.

directly exposed to the primary electrons through the discontinuous part of the skin. For the skeletal tissues (= RBM and endosteum), the ratios are also significantly smaller than unity, by several orders of magnitude in fact. These differences were observed due mainly to the improved representation of the cortical bone in the MRCPs; that is, the cortical bone of the MRCPs is continuous and fully covers the spongiosa and medullary-cavity regions, in contrast to the ICRP-110 phantoms.

3.3.2. *Dose coefficients for effective dose*

Fig. 9 shows the ratios of the DC_E`s of the MRCPs with respect to the ICRP-116 $DC_E$`s for photons and electrons and the irradiation geometries considered in the present study. For photons, it can be seen that the MRCP DC_E`s are generally similar to the ICRP-116 $DC_E$`s, except for very low energies (i.e., 0.01 and 0.15 MeV). The ratios at energies >0.1 MeV are close to unity, having fallen mostly between 0.95 and 1.05. By contrast, the ratios at lower energies show relatively large differences from unity. Except at the lowest energy (0.01 MeV), they tend to be less than unity, because the ratios of MRCP DC_T`s/ICRP-116 $DC_T$`s for the majority of the organs/tissues are less than unity, as shown in Fig. 7. Contrastingly, at 0.01 MeV, the ratios in all of the geometries are greater than unity, with a maximum of approximately 1.7 in the PA geometry. These differences were observed mainly due to the differences from the ICRP-116 skin DC_T`s owing to the skin sensitive region in the MRCPs (see Fig. 7). For electrons, it can be seen that the ratios for energies >1 MeV are close to unity (mostly between 0.95 and 1.05), whereas those for lower energies are significantly different from unity. These significant differences were again observed mainly due to the differences between the MRCP skin DC_T`s and ICRP-116 skin $DC_T$`s, a stemming from the definition of the skin sensitive region in the MCRPs. The ratios of MRCP DC_E`s/ICRP-116 $DC_E$`s can be seen to be almost identical to those of MRCP skin DC_T`s/ICRP-116 skin $DC_T$`s in Fig. 8.

4. Conclusion

In the present study, a complete dataset of dose coefficients (DCs) was calculated for idealized external exposures of photons and electrons using the mesh-type reference computational phantoms (MRCPs) for adult male and female. The dataset provides the dose coefficients for 30 individual organs/tissues (DC_T`s) and the dose coefficients for effective doses ($DC_E$`s) for a wide range of energies, i.e., from 0.01 MeV to 10 GeV, in six irradiation geometries (AP, PA, LLAT, RLAT, ROT, and ISO) for photons and in three geometries (AP, PA, and ISO) for electrons. Subsequently, the DC_T`s for the nine organs/tissues calculated for their thin radiosensitive regions in the MRCPs were compared with those calculated by averaging the absorbed dose over the entire organ/tissue region. The obtained results indicated that the influences of the thin radiosensitive

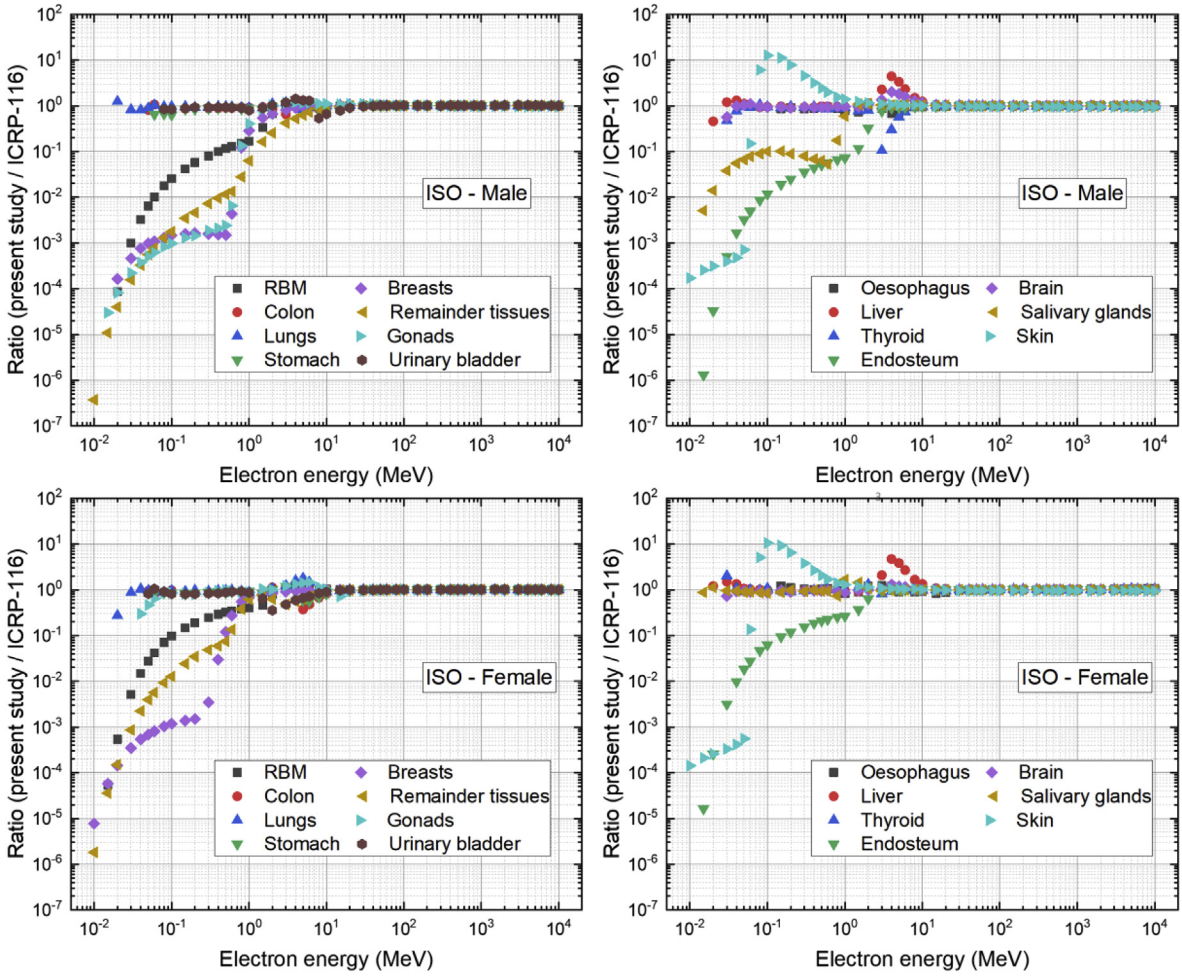

Fig. 8. Ratios of MRCP DC_T`s calculated in present study with respect to ICRP-116 $DC_T$`s (ICRP 2010) for RBM, colon, lungs, stomach, breasts, remainder tissues, gonads, urinary bladder, oesophagus, liver, thyroid, endosteum, brain, salivary glands, and skin for electrons in ISO geometry.

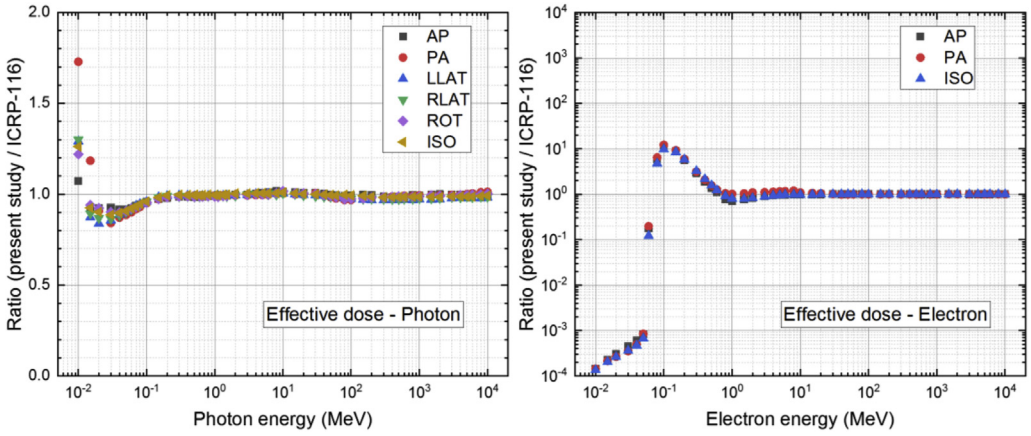

Fig. 9. Ratios of MRCP DC_E`s calculated in present study with respect to ICRP-116 $DC_E$`s (ICRP 2010) for photons (left) and electrons (right).

regions on dose calculations for photons and electrons were generally not significant for most organs/tissues, but very large for the skin and eye lens, especially for electrons. The large influence of the skin sensitive region eventually significantly affected the effective dose calculations for electrons. Additionally, the DCs of the MRCPs were compared with the current reference values in ICRP Publication 116 [2] produced with the voxel-type ICRP-110 reference phantoms [3]. The results showed that for photons, the DC_T`s for the majority of organs/tissues and the $DC_E$`s of the MRCPs were generally similar to the ICRP-116 values, except for very low energies. For electrons, by contrast, significant deviations from the ICRP-116 values were found, particularly for the superficial organs/

tissues and skeletal tissues, and also the DC_E`s, owing mainly to the improved representation of the organs and tissues in the MRCPs as compared with the ICRP-110 phantoms. The comprehensive datasets of the DCs tabulated in a Microsoft Excel spreadsheet are available as Supplemental Data in the journal website. The present study produced the data for photons and electrons, and an additional study will be conducted in the near future for the other particles including neutrons, protons, and helium ions.

Acknowledgments

This project was supported by the Nuclear Safety Research Development (NSR&D) Program through Korea Foundation of Nuclear Safety (KOFONS), funded by the Nuclear Safety and Security Commission, and additionally, by the National Research Foundation of Korea funded by the Ministry of Science, ICT and Future Planning through the National Research Foundation of Korea (Project Nos.: 1705006, 2016R1D1A1A09916337). The work was also funded by the intramural program of the National Institutes of Health, National Cancer Institute, Division of Cancer Epidemiology and Genetics. The contents are solely the responsibility of the authors and do not necessarily represent the official views of the National Institutes of Health. One of the authors (Yeon Soo Yeom) was supported by a grant of the Korean Health Technology R&D Project through the Korean Health Industry Development Institute (KHIDI), funded by the Ministry of Health & Welfare, Republic of Korea (Project No: H18C2257). Two of the authors (Chansoo Choi and Haegin Han) were supported by the Global PhD Fellowship program (Project Nos.: NRF-2017H1A2A1046391, NRF-2018H1A2A1059767). The calculations in this work were performed on the National Institutes of Health's High-Performance Computing Biowulf cluster (http://hpc.nih.gov).

Appendix A. Supplementary data

Supplementary data to this article can be found online at https://doi.org/10.1016/j.net.2018.12.006.

References

[1] ICRP, The 2007 Recommendations of the international commission on radiological protection, ICRP publication 103, Ann. ICRP 37 (2–4) (2007).
[2] ICRP, Conversion coefficients for radiological protection quantities for external radiation exposures, ICRP publication 116, Ann. ICRP 40 (2–5) (2010).
[3] ICRP, Adult reference computational phantoms, ICRP publication 110, Ann. ICRP 39 (2) (2009).
[4] ICRP, Basic anatomical and physiological data for use in radiological protection reference values, ICRP publication 89, Ann. ICRP 32 (3–4) (2002).
[5] R. Behrens, G. Dietze, M. Zankl, Dose conversion coefficients for electron exposure of the human eye lens, Phys. Med. Biol. 54 (2009) 4069–4087.
[6] ICRP, Human respiratory tract model for radiological protection, ICRP publication 66, Ann. ICRP 24 (1–3) (1994).
[7] ICRP, Human alimentary tract model for radiological protection, ICRP publication 100, Ann. ICRP 36 (1–2) (2006).
[8] ICRP, Computational framework for internal dose assessment for reference adults: specific absorbed fractions, ICRP publication 133, Ann. ICRP 45 (2) (2016).
[9] C.H. Kim, Y.S. Yeom, T.T. Nguyen, Z.J. Wang, H.S. Kim, M.C. Han, J.K. Lee, M. Zankl, N. Petoussi-Henss, W.E. Bolch, C. Lee, B.S. Chung, The reference phantoms: voxel vs polygon, Ann. ICRP 45 (S1) (2016) 188–201. https://doi.org/10.1177/0146645315626036.
[10] C.H. Kim, Y.S. Yeom, T.T. Nguyen, M.C. Han, C. Choi, H. Lee, H. Han, B. Shin, J.-K. Lee, H.S. Kim, M. Zankl, N. Petoussi-Henss, W.E. Bolch, C. Lee, B.S. Chung, R. Qiu, K. Eckerman, New mesh-type phantoms and their dosimetric applications, including emergencies, Ann. ICRP 47 (3/4) (2018) 45–62. https://doi.org/10.1177/0146645318756231.
[11] J. Allison, K. Amako, J. Apostolakis, P. Arce, M. Asai, T. Aso, E. Bagulya, S. Banerjee, G. Barrand, B.R. Beck, A.G. Bogdanov, D. Brandt, J.M.C. Brown, H. Burkhardt, Ph Canal, D. Cano-Ott, S. Chauvie, K. Cho, G.A.P. Cirrone, G. Gooperman, M.A. Cortés-Giraldo, G. Cosmo, G. Cuttone, G. Depaola, L. Desorgher, X. Dong, A. Dotti, V.D. Elvira, G. Folger, Z. Francis, A. Galoyan, L. Garnier, M. Gayer, K.L. Genser, V.M. Grichine, S. Guatelli, P. Gueye, P. Gumplinger, A.S. Howard, I. Hřivnáčová, S. Hwang, S. Incerti, A. Ivanchenko, V.N. Ivanchenko, F.W. Jones, S.Y. Jun, P. Kaitaniemi, N. Karakatsanis, M. Karamitros, M. Kelsey, A. Kimura, T. Koi, H. Kurashige, A. Lechner, S.B. Lee, F. Longo, M. Maire, D. Mancusi, A. Mantero, E. Mendoza, B. Morgan, K. Murakami, T. Nikitina, L. Pandola, P. Paprocki, J. Perl, I. Petrović, M.G. Pia, W. Pokorski, J.M. Quesada, M. Raine, M.A. Reis, A. Ribon, A. Ristić Fira, F. Romano, G. Russo, G. Santin, T. Sasaki, D. Sawkey, J.I. Shin, I.I. Strakovsky, A. Taborda, S. Tanaka, B. Tomé, T. Toshito, H.N. Tran, P.R. Truscott, L. Urban, V. Uzhinsky, J.M. Verbeke, M. Verderi, B.L. Wendt, H. Wenzel, D.H. Wright, D.M. Wright, T. Yamashita, J. Yarba, H. Yoshida, Recent developments in Geant4, Nucl. Instrum. Methods Phys. Res. Sect. A Accel. Spectrom. Detect. Assoc. Equip. 835 (2016) 186–225.
[12] Y.S. Yeom, M.C. Han, C.H. Kim, J.H. Jeong, Conversion of ICRP male reference phantom to polygon-surface phantom, Phys. Med. Biol. 58 (2013) 6985–7007.
[13] T.T. Nguyen, Y.S. Yeom, H.S. Kim, Z.J. Wang, M.C. Han, C.H. Kim, J.K. Lee, M. Zankl, N. Petoussi-Henss, W.E. Bolch, C. Lee, B.S. Chung, Incorporation of detailed eye model into polygon-mesh versions of ICRP-110 reference phantoms, Phys. Med. Biol. 60 (2015) 8695–8707.
[14] Y.S. Yeom, H.S. Kim, T.T. Nguyen, C. Choi, M.C. Han, C.H. Kim, J.K. Lee, M. Zankl, N. Petoussi-Henss, W.E. Bolch, C. Lee, B.S. Chung, New small-intestine modeling method for surface-based computational human phantoms, J. Radiol. Prot. 36 (2016) 230–245.
[15] Y.S. Yeom, Z.J. Wang, T.T. Nwguyen, H.S. Kim, C. Choi, M.C. Han, C.H. Kim, J.K. Lee, B.S. Chung, M. Zankl, N. Petoussi-Henss, W.E. Bolch, C. Lee, Development of skeletal system for mesh-type ICRP reference adult phantoms, Phys. Med. Biol. 61 (2016) 7054–7073.
[16] H.S. Kim, Y.S. Yeom, T.T. Nguyen, C. Choi, M.C. Han, J.K. Lee, C.H. Kim, M. Zankl, N. Petoussi-Henss, W.E. Bolch, C. Lee, U. Qiu, K. Eckerman, B.S. Chung, Inclusion of thin target and source regions in alimentary and respiratory tract systems of mesh-type ICRP adult reference phantoms, Phys. Med. Biol. 62 (2017) 2132–2152.
[17] Y.S. Yeom, H. Han, C. Choi, T.T. Nguyen, H. Lee, B. Shin, C.H. Kim, M.C. Han, Calculation of local skin doses with ICRP adult mesh-type reference computational phantoms, J. Kor. Phys. Soc. 72 (2018) 177–182.
[18] H. Si, TetGen, a Delaunay-based quality tetrahedral mesh generator, ACM Trans. Math Software 41 (2015) 11, 1–11:36.
[19] Y.S. Yeom, J.H. Jeong, M.C. Han, C.H. Kim, Tetrahedral-mesh-based computational human phantom for fast Monte Carlo dose calculations, Phys. Med. Biol. 59 (2014) 3173–3185.
[20] P.B. Johnson, A.A. Bahadori, K.F. Eckerman, C. Lee, W.E. Bolch, Response functions for computing absorbed dose to skeletal tissues from photon irradiation—an update, Phys. Med. Biol. 56 (2011) 2347–2365.